water

MDPI

Article

Optimization of a Snow and Ice Surface Albedo Scheme for Lake Ulansu in the Central Asian Arid Climate Zone

Xiaowei Cao [1,*], Miao Yu [2], Puzhen Huo [2], Peng Lu [2], Bin Cheng [3], Wei Gao [1], Xingyu Shi [1] and Lijun Wang [4,*]

[1] School of Architectural Engineering, Qingdao Huanghai University, Qingdao 266555, China; gaow@qdhhc.edu.cn (W.G.); shixy11@qdhhc.edu.cn (X.S.)
[2] State Key Laboratory of Coastal and Offshore Engineering, Dalian University of Technology, Dalian 116023, China; yumiao2411@dlut.edu.cn (M.Y.); hpz_ice@mail.dlut.edu.cn (P.H.); lupeng@dlut.edu.cn (P.L.)
[3] Finnish Meteorological Institute, 00101 Helsinki, Finland; bin.cheng@fmi.fi
[4] Huacheng Boyuan Engineering Technology Group Co., Ltd., Beijing 100043, China
* Correspondence: caoxw11@qdhhc.edu.cn (X.C.); 13901212966@sina.cn (L.W.)

Abstract: Surface albedo measurements of snow and ice on Lake Ulansu in the Central Asian arid climate zone were conducted during the winter of 2016–2017. Observations were categorized into three stages based on the ice growth and surface condition: bare ice, snow cover, and melting. During the bare ice stage, the mean surface albedo was 0.35 with a decreasing trend due to the accumulation of wind-blown sediment on the ice surface (range: 0.99–1.87 g m^{-2}). Two snowfall events occurred during the snow cover stage, significantly increasing the surface albedo to 0.91. During the melting stage, the albedo decreased at a decay rate of 0.20–0.30/day. Four existing albedo schemes were evaluated but found unsuitable for Lake Ulansu. A new surface albedo scheme was proposed by incorporating the existing albedo schemes with the measured data. This scheme incorporated the effect of sediment content on bare ice albedo for the first time. It demonstrated a modelling efficiency of 0.933 over the entire 3-month period, which was used to evaluate the fit between the predicted and observed values. When validated with albedo observations from other winters, it achieved a modelling efficiency of 0.940. The closer the value is to 1, the better the model's predictive accuracy, indicating a higher level of reliability in the model's performance. This scheme has potential applicability to other lakes in the Central Asian arid climate zone, which is characterized by low precipitation, frequent sandstorms, and intense solar radiation.

Keywords: albedo scheme; lake ice; snow; sediment content; optimization

check for updates

Academic Editor: Hung Tao Shen

Received: 25 December 2024
Revised: 22 January 2025
Accepted: 26 January 2025
Published: 12 February 2025

Citation: Cao, X.; Yu, M.; Huo, P.; Lu, P.; Cheng, B.; Gao, W.; Shi, X.; Wang, L. Optimization of a Snow and Ice Surface Albedo Scheme for Lake Ulansu in the Central Asian Arid Climate Zone. *Water* **2025**, *17*, 523. https://doi.org/10.3390/w17040523

Copyright: © 2025 by the authors. Licensee MDPI, Basel, Switzerland. This article is an open access article distributed under the terms and conditions of the Creative Commons Attribution (CC BY) license (https://creativecommons.org/licenses/by/4.0/).

1. Introduction

Lake ice and snow albedo, which refers to the fraction of solar energy reflected by these surfaces, have a substantial impact on the energy balance of lakes and their surrounding environments [1–6]. Seasonal ice-covered lakes are a key component of the terrestrial landscape in the Northern Hemisphere [7,8]. Due to rising global air temperatures, numerous studies have reported a significant reduction in the annual freezing period of lakes [7,9–11]. Predictive studies on Northern Hemisphere temperatures indicate that the duration of seasonal ice cover will continue to decrease in the future [12–14]. This reduction in lake ice during winter can significantly impact water resources, ecological stability, transportation, fisheries, and human activities [15]. The Central Asian arid climate zone plays a critical

role in the global climate system [16], with warming rates in this region occurring at a pace faster than the global average [17]. This has further exacerbated the reduction of seasonal lake ice in the zone [18]. When studying lake ice and snow in this area, it is essential to consider its unique climatic characteristics, such as low precipitation (approximately 8 mm during the winter), frequent sandstorms (approximately 15 days per year), and intense solar radiation (approximately 200 W/m^2 during the freezing period) [3,19–21]. For winter lake ice surfaces, two main conditions exist: with snow cover and without. Key factors affecting snow cover albedo include snow water content, impurity level [22], grain size [23], snow density, and surface roughness [24,25]. Dry snow has an albedo as high as 0.9 that decreases with increasing liquid water, while for wet snow, it is typically around 0.5 [26–28]. Factors affecting the albedo of lake ice include the presence of air bubbles within the ice, ice crystal structure, ice thickness, and surface roughness [29]. Dry ice has an albedo of approximately 0.5, decreasing to 0.2–0.3 during the melting season [3,8]. Many existing snow and ice albedo schemes are empirical and rely on easily obtainable climatic data [30–33]. These schemes typically estimate snow albedo using parameters such as snow depth and the number of days since snowfall [30,34] and estimate lake ice albedo using ice thickness and surface temperature [35–37]. While these parameterizations offer reasonable approximations of snow and ice albedo, their applicability is limited. They rely on the statistical fitting of albedo measurements that reflect specific snow, ice, and atmospheric conditions at particular times and locations [38]. These parameterization schemes are primarily applied to high-latitude lakes and do not take into account the climatic characteristics of the Central Asian arid climate zone. Additionally, these schemes have not been validated for lake ice and snow in this particular region.

In summary, although lake ice albedo in the Central Asian arid climate zone plays an important role in climate system studies, a snow and ice albedo scheme for its entire ice period is lacking. In this study, a field investigation was conducted to measure the snow and ice cover albedo of a typical lake (Lake Ulansu [3,18,39]) in the Central Asian arid climate zone and to validate existing snow and ice albedo schemes. Additionally, a new snow and ice albedo scheme was optimized by refining the existing schemes and incorporating climatic characteristics and the measured data. The accuracy of the new scheme was further validated using 3 years of winter surface albedo measurements.

2. Materials and Methods

2.1. Study Area

Lake Ulansu is located in Inner Mongolia, China at coordinates 40°36′–41°30′ N, 108°43′–108°70′ E. It covers an area of 306 km^2, with maximum length and width of 35.4 km and 12.7 km, respectively. The water volume of the lake can reach 2.5–3 × 10 m^3 [40], and the maximum and mean water depths are 2.5–3.0 and 1.0–1.5 m [18], respectively. Existing survey results show that the maximum ice thickness in winter ranges from 0.3 to 0.6 m [17,40,41]. This field study was conducted from 1 January to 9 March in 2017 in the eastern part of the lake (40.9° N, 108.9° E), approximately 200 m from the shore (Figure 1). The water depth at the observation point was 1.7 m, and the maximum ice thickness was 0.57 m, both of which fall within the average range for the Lake Ulansu during the winter and are representative.

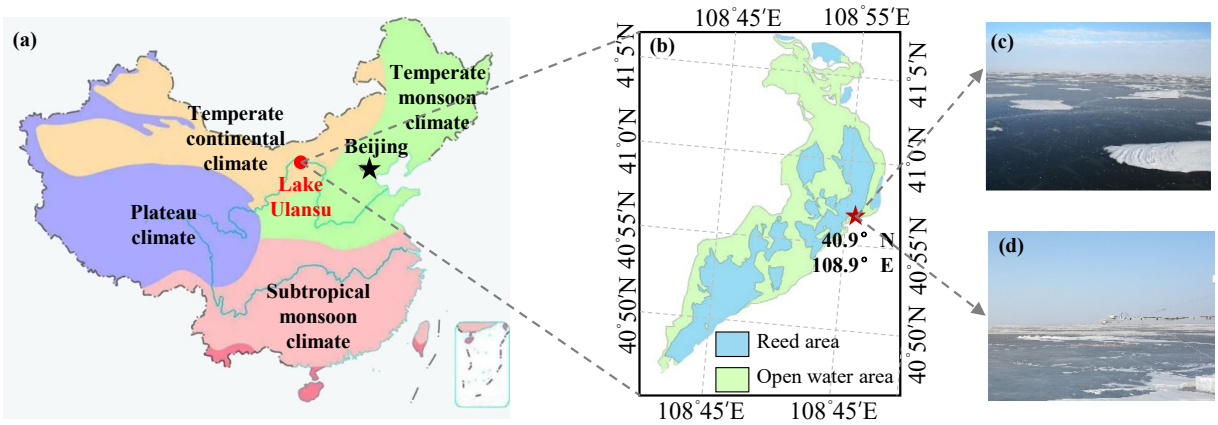


Figure 1. Location of Lake Ulansu (**a**) [18], measurement site (Universal Transverse Mercato projection and plotted using QGIS (Quantum GIS 3.34)) (**b**), ice cover on the lake (**c**), and solar radiation measurement (**d**).

2.2. Data Collection

In situ measurements of solar radiation, atmospheric surface layer conditions (temperature, humidity, and wind speed and direction), and snow and ice thickness were conducted. Figure 2 illustrates the equipment used to measure solar radiation and atmospheric conditions, with further details provided in a previous study [39]. Solar radiation was measured using two pyranometers (TBQ-2, Jinzhou Sunshine Meteorological Technology Co., Ltd., Jinzhou, China, http://pvsb.china-nengyuan.com/member_product/78658.html, accessed on 1 January 2017.): one for incoming radiation and one for reflected radiation. The TBQ-2 measurement range was 300–3000 nm, with a sensor accuracy of 5%, and its manufacturing and calibration standards followed the guidelines specified in QX/T 55-2007.

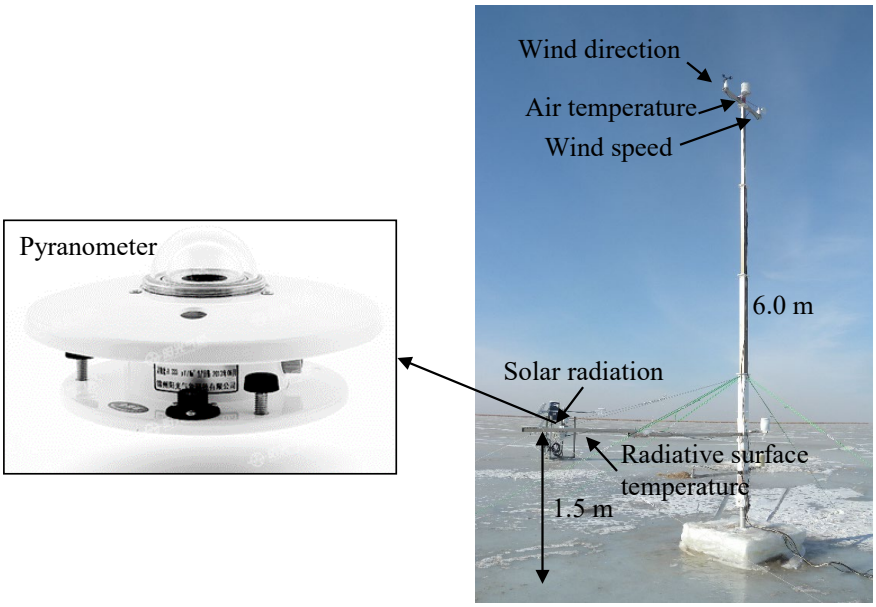


Figure 2. Meteorological tower measurements at the site, and the pyranometers used, in winter 2016–2017.

In arid and semi-arid regions, environmental conditions often result in the adherent of a layer of sediment to the lake ice surface. To quantify the sediment content, the sediment per unit area was measured. A 0.5 × 0.5 m area was delineated on the ice surface (Figure 3), and surface sediment was collected from this area. The sediment was then dried and

weighed to calculate its content per unit area (g m^{-2}), following the procedures outlined in the GB11901–1989 standard [42]. The detailed steps are as follows:

1. Place the filter membrane in a drying oven and dry it at a temperature of 103–105 °C for 2 h. Remove it and place it in a desiccator to cool to room temperature, then weigh it to obtain the net weight of the filter membrane.
2. Press the filter membrane tightly against the inner wall of the funnel. Using a vacuum filtration method, filter the water sample containing surface sediment.
3. After filtration, the sediment will adhere to the filter membrane. Place the filter membrane back into the drying oven and dry it again at the same temperature for 2 h. Remove it and place it in a desiccator to cool to room temperature, then weigh it to obtain the total weight of the filter membrane and the sediment.
4. Subtract the net weight of the filter membrane from the total weight to obtain the weight of the sediment.

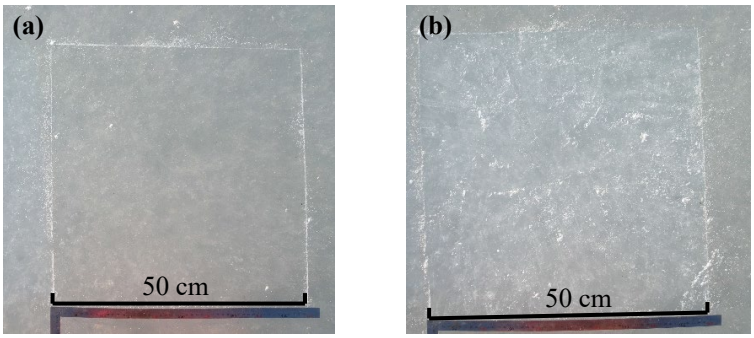


Figure 3. Sediment collection area: pre- (**a**) and post-collection (**b**).

Sediment content measurements were taken daily during the snow-free observation stage, with each day's sampling location adjacent to the previous day's location.

2.3. Existing Surface Albedo Schemes

Albedo schemes previously applied to predict lake ice and snow albedo were selected. These included those proposed by Gabison [36], Shine and Henderson-Sellers (SH), Flato and Brown (FB) [35], and Henneman and Stefan (HS) [30].

2.3.1. Gabison Scheme

The Gabison scheme, developed based on the method suggested by Maykut [35] and combined with field measurement data, requires parameters such as ice and snow thickness and surface temperature. Albedo calculations are divided into two stages based on ice surface temperature: freezing ($T_s \leq -3$ °C) and melting ($T_s \geq -3$ °C) stages. During the freezing stage, the albedo of the ice surface (α_i) is derived using quadratic regression with respect to ice thickness (h_i), and is within the range 0.05 m $\leq h_i \leq$ 1 m.

$$\alpha_i = 0.21 + 1.026h_i - 0.561h_i^2, \quad (1)$$

The albedo of snow (α_s) is calculated based on the ice albedo and snow thickness:

$$\alpha_s = \alpha_i + (0.8 - \alpha_i)\frac{h_s}{0.05}, \quad (2)$$

where h_s is the depth of the snow cover.

During the melting stage, the albedo of ice with a thickness of 1 m or more decreases linearly from 0.72 to 0.47. A similar linear decrease is applied to thinner ice (0.05 m $\leq h_i \leq$ 1 m) during the melting stage (Figure 4).

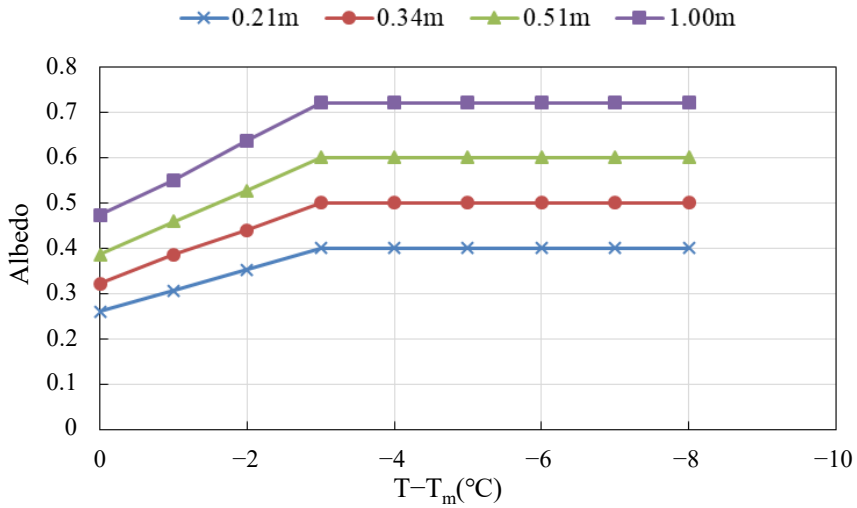


Figure 4. Dependence of ice albedo on ice thickness and melting temperature deficit [36].

2.3.2. Shine and Henderson-Sellers (SH) Scheme

Shine and Henderson-Sellers summarized previous albedo schemes and proposed new schemes for different ice surface types. These schemes require parameters such as snow depth and ice thickness. The specific classifications and calculation formulas are presented in Table 1.

Table 1. Shine and Henderson-Sellers scheme.

Albedo Class	Value
Dry snow	$\alpha_s = 0.8$
Melting snow	$\alpha_s = 0.65$
Thin melting snow on bare ice ($h_s \leq 0.1$ m)	$\alpha_s = 0.53 + 1.2h_s$
Bare ice ($h_i \geq 1.5$ m)	$\alpha_i = 0.53$
Thin melting ice ($1.5 \geq h_i \geq 0$ m)	$\alpha_i = 0.47 + 0.21(h_i - 1.0)$, $1.5 \geq h_i \geq 1.0$ m $\alpha_i = 0.25 + 0.70h_i - 0.86h_i^2 + 0.38h_i^3$, $1.0 \geq h_i \geq 0.05$ m $\alpha_i = 0.1 + 3.6h_i$, $h_i \leq 0.05$ m
Thin forming ice ($1.5 \geq h_i \geq 1.0$ m)	$\alpha_i = 0.47 + 0.50(h_i - 1.0)$, $1.0 \geq h_i \geq 0.05$ m $\alpha_i = 0.25 + 0.70h_i - 0.86h_i^2 + 0.38h_i^3$, $1.0 \geq h_i \geq 0.05$ m $\alpha_i = 0.1 + 3.6h_i$, $h_i \leq 0.05$ m
Bare frozen ice ($h_i \geq 1.5$ m)	$\alpha_i = 0.72$
Snow on frozen ice	$\alpha_s = 0.8$, $h_s \geq 0.5$ m $\alpha_s = \alpha_i + \frac{h_s(0.8-\alpha_i)}{0.05}$, $h_s \leq 0.5$ m; $h_i \leq 1.5$ m

2.3.3. Flato and Brown (FB) Scheme

In the FB scheme, the freezing ice albedo is derived from Maykut [43], while the melting ice albedo is based on Heron and Woo [44]. Surface temperature (T_s) is incorporated, and ice and snow are classified into two types (freezing and melting) based on the surface temperature.

$$\text{Albedo} = \begin{cases} \min[\alpha_s,\ \alpha_i + h_s(\alpha_s - \alpha_i)/0.1] & h_i > 0.001 \text{ m}\ \ h_s < 0.1 \text{ m} \\ \alpha_s & h_i > 0.001 \text{ m}\ \ h_s > 0.1 \text{ m} \end{cases}, \quad (3)$$

$$\begin{cases} \alpha_i = \max\left(0.15,\ 0.44h_i^{0.28} + 0.08\right) \\ \alpha_s = 0.75 \end{cases}, \ T_s < 0\ ^\circ\mathrm{C}, \quad \begin{cases} \alpha_i = \min\left(0.55,\ 0.075h_i^{2} + 0.15\right) \\ \alpha_s = 0.65 \end{cases}, \ T_s = 0\ ^\circ\mathrm{C}, \tag{4}$$

2.3.4. Henneman and Stefan (HS) Scheme

The HS scheme improves upon the FB snow albedo scheme by calculating snow albedo based on accumulated solar radiation and air temperature. It introduces parameters such as accumulated solar radiation, air temperature, and the number of days since the last snowfall. The accumulation of solar radiation and air temperature is reset with each new snowfall day, which is defined as a day on which snowfall exceeds 2.5 mm (i.e., a snowfall greater than a trace amount).

Accumulated solar radiation is the sum of daily radiation received from the time of a new snowfall until the next snowfall day. Accumulated air temperature is calculated using a degree–day method with a calibrated base temperature, T_{base}. A temperature index, T_{index}, for each day is computed as:

$$T_{index} = T_a - T_{base}, \tag{5}$$

where T_a is the average daily air temperature (°C) and $T_{base} = -18$°C.

Scheme I:

This requires inputs such as average daily air temperature, accumulated solar radiation, accumulated air temperature, and daily snowfall data.

For the freezing stage, the α_s is given by:

$$\alpha_s = -0.0015R + 0.83, \tag{6}$$

For the melting stage, the α_s is given by:

$$\alpha_s = \begin{cases} 0.0029R - 0.009T + 0.95, & T_a \geq 0\ ^\circ\mathrm{C} \\ \alpha_{s_{-1}} - 0.00036T + 0.95, & T_a < 0\ ^\circ\mathrm{C} \end{cases}, \tag{7}$$

where R is accumulated incoming daily solar radiation since the last snowfall (MJ m^{-2}), $\alpha_{s_{-1}}$ is the albedo on the previous day, and T is the accumulated daily air temperature index since the last snowfall (°C).

Scheme II:

This requires only snowfall and average air temperature data to predict the albedo.

For the freezing stage, the α_s is calculated as:

$$\alpha_s = -0.011d + 0.83, \tag{8}$$

For the melting stage, the α_s is given by:

$$\text{Melting stage: } \alpha_s = \begin{cases} \alpha_{s_{-1}} - 0.17, & T_a \geq 0\ ^\circ\mathrm{C} \\ \alpha_{s_{-1}} - 0.013, & T_a < 0\ ^\circ\mathrm{C} \end{cases}, \tag{9}$$

where d is the number of days since the last snowfall.

The input parameters, output albedo, and a brief analysis of each scheme are presented in Table 2. From the table, it is evident that none of these schemes consider the effect of sediment content on the albedo of the ice surface. Therefore, the accuracy of their albedo calculations for the ice and snow on Lake Ulansu remains to be validated.

Table 2. Summary of existing albedo schemes.

Albedo Scheme	Input Parameters	Output Albedo	Analysis
Gabison	Ice surface temperature; Ice thickness; Snow thickness	Ice and snow	Does not provide a calculation formula for snow albedo during the melting period.
SH	Ice thickness; Snow thickness	Ice and snow	For snow albedo greater than 0.5 m, only reference values are provided, without considering variations in snow properties.
FB	Ice surface temperature; Ice thickness; Snow thickness	Ice and snow	Similar to the SH scheme, the snow albedo is provided only as a reference, without accounting for variations in snow properties.
HS I	Accumulated solar radiation; Accumulated air temperature	Snow	The acquisition of cumulative temperature and radiation is challenging.
HS II	Days since last snowfall; Average air temperature	Snow	The calculation is relatively simple, but it can only calculate the snow albedo.

3. Results of Existing Schemes

3.1. General Ice Conditions

Figure 5 presents the observed data on incident and reflected solar radiation, average albedo, ice and snow thickness, and daily average air temperature from 1 January to 6 March 2017 on Lake Ulansu. The average daily albedo was calculated by dividing the total daily reflected solar radiation by the total daily incoming solar radiation [30]. The total daily solar radiation was obtained by integrating 10-minute radiation measurements over daylight hours.

Based on the ice and snow thickness data shown in Figure 5a, the observation stage was divided into three distinct phases:

1. Bare ice stage (1 January to 6 February):

During this phase, the ice thickness increased from 33.2 to 50.9 cm, with an average growth rate of 0.49 cm/day. Sediment content on the lake ice surface was measured throughout this stage.

2. Snow cover stage (7 February to 3 March):

During this stage, the ice thickness increased from 50.9 cm to its maximum thickness of 56.9 cm. Two snowfall events occurred in this stage: on 7 February and 21 February. Following the first snowfall, snow thickness decreased from 13 cm to <1 cm within a week. The second snowfall was limited to 2.3 cm and had melted completely by 3 March.

3. Melting stage (4 March to 9 March):

In this stage, the ice thickness decreased from 56.9 to 54.2 cm, with a melting rate of 0.4 cm/day.

Throughout the observation stage, the average sediment content was 1.39 ± 0.21 g m^{-2}, exhibiting a clear increasing trend, with a regression coefficient of 0.02. The average incident and reflected solar radiation were 91.75 and 49.89 W m^{-2}, respectively. During the snow-free freezing stage, the average reflected solar radiation was approximately 58.3 W m^{-2}. Following the snowfalls on 7 February and 21 February, the average reflected irradiance exceeded 200 W m^{-2}, subsequently decreasing as the snow melted. The albedo changes followed the same trend as the reflected solar radiation.

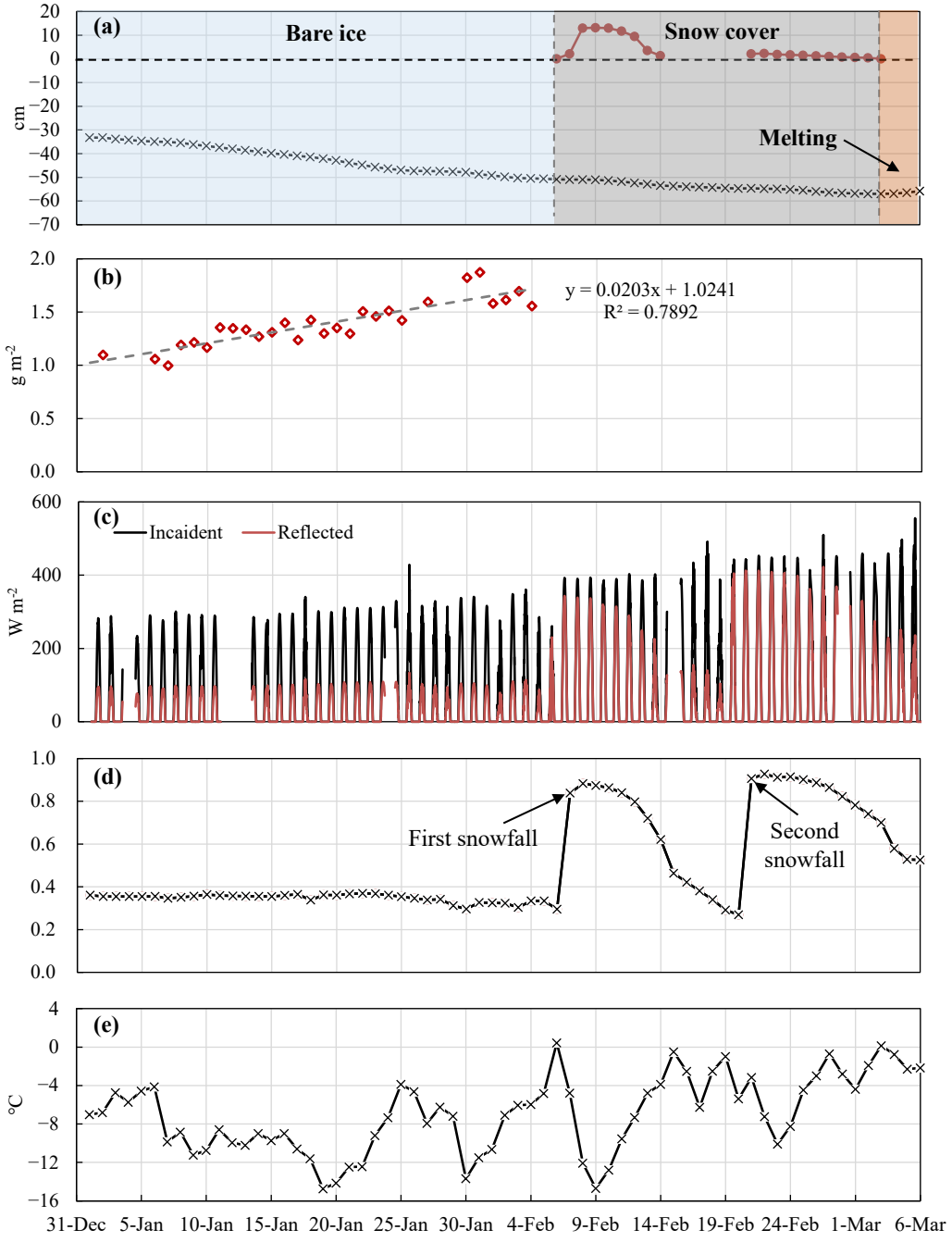


Figure 5. (**a**) Snow and ice thickness, (**b**) sediment content before snowfall, (**c**) incident and reflected solar radiation, (**d**) average albedo, and (**e**) daily average air temperature between 1 January and 6 March 2017.

In the freezing stage, the average albedo was 0.35 ± 0.02. After each snowfall, the albedo increased to approximately 0.91, then gradually decreased as the snow melted. During the melting stage, the average albedo was 0.55 ± 0.07. The average daily air temperature during the observation stage was −6.74 ± 3.95 °C, with the daily average temperature ranging from a maximum of 0.44 °C to a minimum of −14.73 °C.

3.2. Prediction Results for Different Stages

Using the albedo schemes described in Section 2.3, the observational data from Figure 5 were applied to predict the albedo. To assess the accuracy of the predictions, several error analysis metrics were used, including the mean absolute error (MAE), root mean square

error (RMSE), mean absolute percentage error (MAPE), and modeling efficiency (EF). These coefficients provide a comprehensive evaluation of scheme performance. The EF serves as an overall indicator of the goodness of fit, with values closer to 1 indicating a better fit between the predicted and observed results. The specific calculation formulas for these metrics are provided in Appendix A.

3.2.1. Bare Ice Stage

The predicted albedo values for the bare ice stage are shown in Figure 6. The SH and FB schemes provided predictions closer to the observed values, while the Gabison scheme predictions exhibited a larger deviation, mainly due to a higher initial albedo value. All three schemes predicted a gradual increase in albedo, in contrast to the observed trend. Table 3 presents the error analysis of the scheme predictions relative to the observed data. According to this analysis, the SH scheme yielded the most accurate results, with MAE, RMSE, MAPE, and EF values of 0.073, 0.078, 21.471%, and −14.574, respectively. Although this scheme provided the closest fit, it still did not meet the required error analysis standards. Specifically, an EF value less than zero indicates that the scheme is not suitable for simulation. All EF values were negative because all predicted values were higher than the observed values. This discrepancy is attributed to the presence of sediment on the ice surface of Lake Ulansu, which reduces albedo compared to that on typical high-latitude lakes [3]. Therefore, none of these three schemes were appropriate for predicting albedo during the bare ice stage at Lake Ulansu.

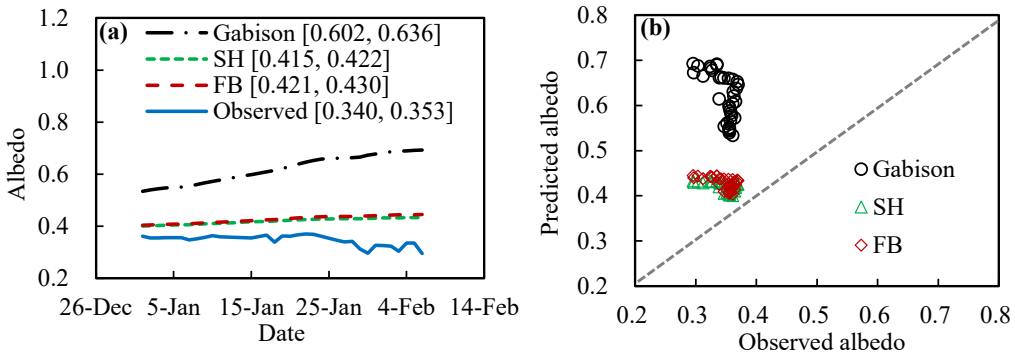


Figure 6. Albedo values observed and predicted by the Gabison, Shine and Henderson-Sellers (SH), and Flato and Brown (FB) schemes during the bare ice stage (**a**), with 95% confidence intervals in brackets, and the comparison between predicted and observed albedo (**b**).

Table 3. Mean absolute error (MAE), root mean square error (RMSE), mean absolute percent error (MAPE), and modeling efficiency (EF) for the Gabison, SH, and FB schemes during the bare ice stage.

Statistical Parameter	Gabison	SH	FB
MAE	0.273	0.073	0.080
RMSE	0.281	0.078	0.085
MAPE	79.866%	21.471%	23.506%
EF	−203.179	−14.574	−17.662

3.2.2. Snow Cover Stage

During the snow cover stage, the HS scheme (Equations (6) and (7)) was also incorporated. As shown in Figure 7, all schemes captured the general increasing and decreasing albedo trends following snowfall. However, the albedo predictions from the FB and Gabison schemes exhibited larger deviations, primarily due to unrealistic initial value settings. The SH scheme predicted a decline in albedo that was too rapid, with both the minimum and maximum values deviating to some extent from the observed data. Among

the two HS scheme variants, scheme II provided predictions that aligned more closely with the observed data than those of scheme I. However, the minimum albedo value predicted by scheme II approached 0, which is significantly lower than the observed minimum value of 0.26.

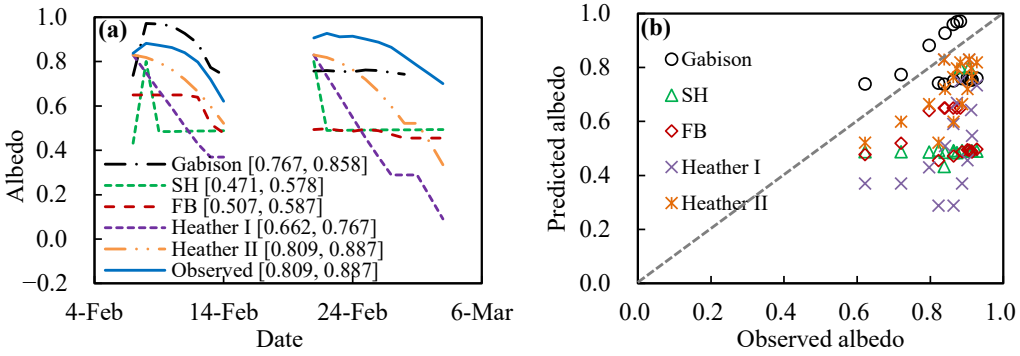


Figure 7. Albedo values observed and predicted by the Gabison, SH, FB, and Hennemen and Stefan (HS) I and II schemes during the snow cover stage (**a**), with 95% confidence intervals in brackets, and the comparison between predicted and observed albedo (**b**).

The error analysis results in Table 4 show that SH scheme II produced the smallest deviation from the observed values. The EF values for SH, FB, and HS I were all less than 0, indicating that they were unsuitable for predicting snow albedo on Lake Ulansu during winter. Although the EF value for the Gabison scheme was greater than 0, it remained lower than that of HS II. From the observation results, it can be seen that the albedo increased to 0.91 after snowfall and then gradually decreased as the snow melted. Notably, the second snowfall was about 8 cm less than the first, which indicates a low correlation between snow depth variation and albedo reduction in Lake Ulansu. Consequently, the prediction results from the Gabison, SH, and FB schemes, which rely on snow depth to calculate albedo, are less accurate. On the other hand, the HS I scheme relies on cumulative temperature and radiation for its calculations. However, the temperature and cumulative radiation in Lake Ulansu differ significantly from those in high-latitude lakes, making the HS I scheme less accurate than the HS II scheme.

Table 4. MAE, RMSE, MAPE, and EF for the Gabison, SH, FB, and HS schemes during the snow cover stage.

Statistical Parameter	Gabison	SH	FB	HS I	HS II
MAE	0.180	0.271	0.244	0.281	0.137
RMSE	0.220	0.303	0.279	0.314	0.155
MAPE	39.040%	38.600%	33.682%	43.583%	23.620%
EF	0.108	−0.740	−0.478	−0.874	0.546

3.2.3. Melting Stage

For the melting stage, the albedo results (Figure 8) indicated that the FB and SH schemes were numerically closer to the measured values than the Gabison scheme. However, all three schemes significantly diverged from the observed trend. This was confirmed by the error analysis in Table 5, which shows that the EF values for all schemes were below 0, indicating that none of these were suitable for simulating ice albedo on Lake Ulansu during the melting stage.

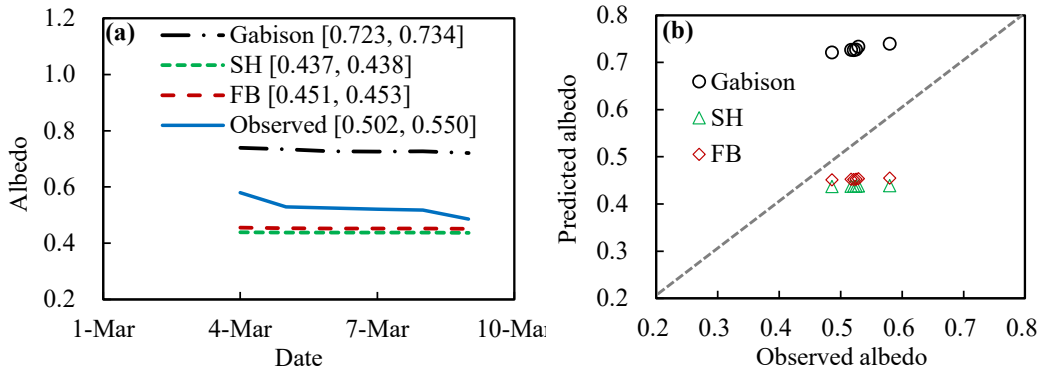


Figure 8. Albedo values observed and predicted by the Gabison, SH, and FB schemes during the snow melting stage (**a**), with 95% confidence intervals in brackets, and the comparison between predicted and observed albedo (**b**).

Table 5. MAE, RMSE, MAPE, and EF for the Gabison, SH, and FB schemes during the melting stage.

Statistical Parameter	Gabison	SH	FB
MAE	0.144	0.160	0.144
RMSE	0.167	0.191	0.178
MAPE	27.111%	24.635%	22.001%
EF	−1.515	−2.276	−1.839

4. A New Albedo Scheme Based on Observations

4.1. New Albedo Scheme Development

Based on the results from Section 3.2, a new albedo scheme for lake ice and snow was optimized for the bare ice, snow cover, and melting stages.

4.1.1. Bare Ice Stage

As shown in Figure 5, while the scheme predictions were relatively close to the measured values, they exhibited an opposite trend compared to the observed data. This discrepancy was primarily due to the sediment layer on the ice surface, which showed a clear increasing trend (Figure 5). To address this, the effect of surface sediment content on albedo was incorporated into the parameterization for the bare ice stage. Based on the error analysis in Table 2, the SH scheme was selected for optimization during this stage. In the SH scheme, albedo is calculated using ice thickness as the primary parameter. Given that changes in ice thickness closely align with variations in surface sediment content, a linear fit of ice thickness (h_i) and surface sediment content (G_s) was performed using the least squares method. The resulting formula is shown in Equation (10), with the fitting results presented in Figure 9.

$$G_s = -0.13 + 3.56h_i, \quad (10)$$

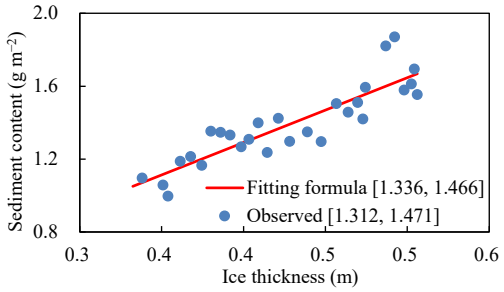


Figure 9. Fitting result of the ice thickness and sediment content before snowfall, with 95% confidence intervals in brackets.

Figure 9 shows the linear fit between ice thickness and sediment content prior to snowfall. The fit was highly accurate, with an EF value of 0.778. Using the sediment content and ice thickness data, a least squares method was applied to develop the albedo scheme, resulting in a best-fitting equation of (11):

$$\alpha_i = -0.10 - 0.18 \times h_i + 0.49 \times G_s - 0.18 \times G_s^2, \quad (11)$$

By combining Equations (10) and (11), the albedo scheme for the bare ice stage of Lake Ulansu was derived as:

$$\alpha_i = \max\left(0.2, 0.03 + 1.74 \times h_i - 2.29 \times h_i^2\right),\ 0 < h_i \leq 0.60\ \text{m}, \quad (12)$$

The predicted albedo results, shown in Figure 10, demonstrated that after adjusting the formula coefficients to incorporate surface sediment content, the calculated albedo trend aligned well with the observed data, and the values also closely matched. The error analysis further revealed that the adjusted scheme provided satisfactory results, with an MAE of 0.009, RMSE of 0.012, MAPE of 2.748%, and EF of 0.695.

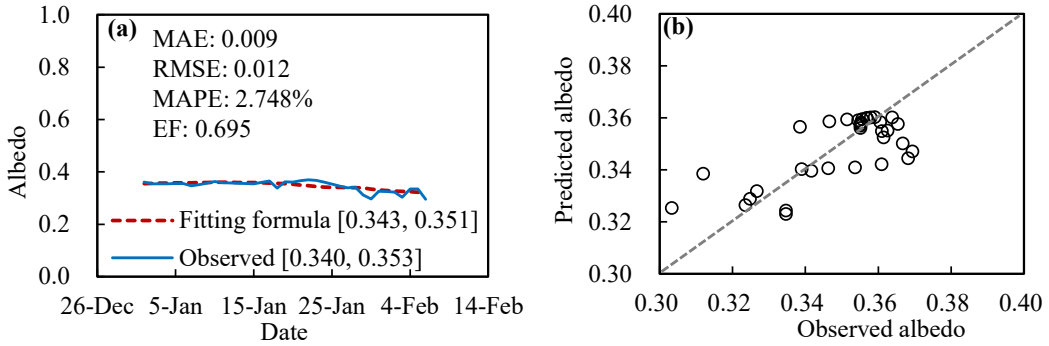


Figure 10. Observation and fitting results of the albedo during the bare ice stage (**a**), with 95% confidence intervals in brackets, and the predicted vs. observed albedo (**b**).

4.1.2. Snow Cover Stage

The main factors influencing snow albedo are snow thickness and its physical properties. As shown in Figure 5a,d, although the snow thickness varied by 8 cm between the two snowfall events, the albedo consistently increased to 0.91 after each snowfall. This suggests that the impact of snow thickness on snow cover albedo at Lake Ulansu is relatively small. Based on the error analysis in Figure 7 and Table 3, the HS II scheme, using the number of days since snowfall as a key parameter, showed the best performance in terms of both trend accuracy and error metrics. Therefore, the HS II scheme was selected for optimization, and the number of days since snowfall was used for parabolic fitting, as shown in Equation (13):

$$\alpha_s = \max\left(0.4, 0.884 + 0.025 \times d - 0.004 \times d^2\right),\ h_s > 0\ \text{m}, \quad (13)$$

The albedo prediction results are shown in Figure 11. The optimized albedo scheme for the snow cover stage accurately captured the trend of albedo changes following snowfall and was numerically close to the observed values, with an EF of 0.796.

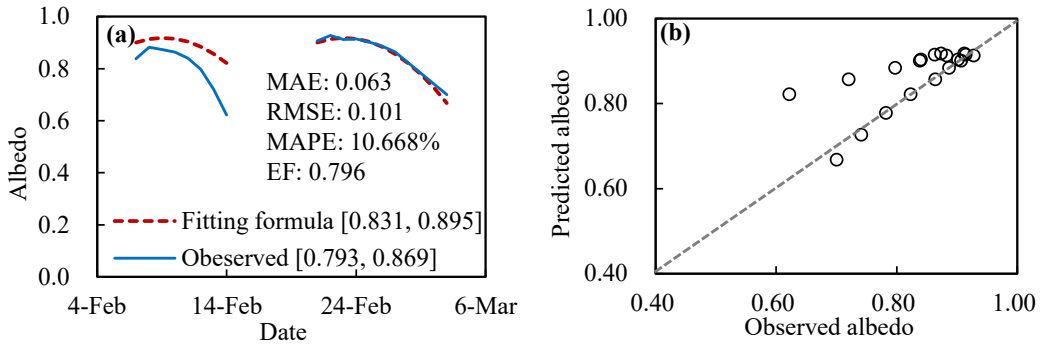


Figure 11. Observation and fitting results of the albedo during the snow cover stage (**a**), with 95% confidence intervals in brackets, and the predicted vs. observed albedo (**b**).

4.1.3. Melting Stage

As discussed in Section 3.2.3, the existing albedo schemes produced unsatisfactory results for calculating albedo during the ice melting stage on Lake Ulansu. Based on the bare ice stage, the albedo during the melting stage was re-fitted as a function of ice thickness, as shown in Equation (14):

$$\alpha_i = \max\left(0.1, -0.25 + 1.40h_i\right),\ 0\ \text{m} < h_i \leq 0.60\ \text{m}, \tag{14}$$

The results, shown in Figure 12, demonstrated that the re-fitted scheme yielded satisfactory calculation results in both trend and numerical values. The error analysis also showed positive results, with a MAE of 0.012, RMSE of 0.018, MAPE of 2.402%, and EF of 0.531.

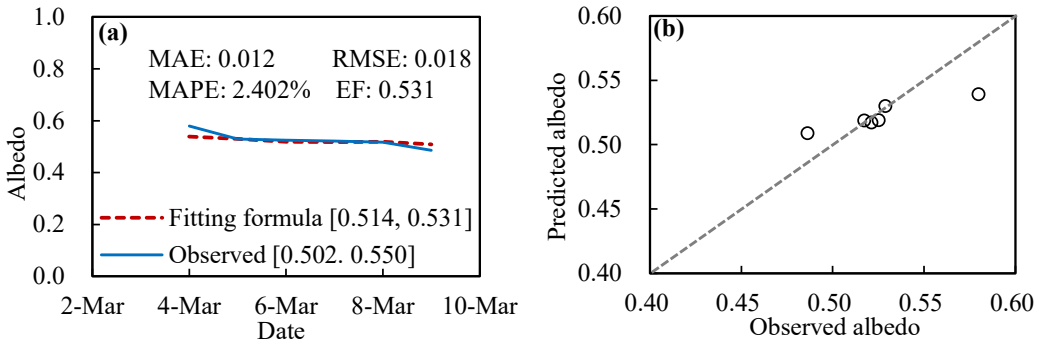


Figure 12. Observation and fitting results of the albedo during the melting stage (**a**), with 95% confidence intervals in brackets, and the predicted vs. observed albedo (**b**).

4.1.4. Whole Observation Stage

By integrating the scheme optimization results from the three stages with the field measurement data, the lake ice albedo scheme for Lake Ulansu was summarized, as shown in Equation (14).

Bare ice stage:

$$\alpha_i = \max\left(0.2, 0.03 + 1.74 \times h_i - 2.29 \times h_i^2\right),\ 0 < h_i \leq 0.60\ \text{m},$$

Snow cover stage:

$$\alpha_s = \max\left(0.4, 0.884 + 0.025 \times d - 0.004 \times d^2\right),\ h_s > 0\ \text{m},$$

Melting stage:

$$\alpha_i = \max(0.1, -0.25 + 1.40h_i),\ 0 < h_i \leq 0.60\ \text{m},$$

Figure 13 shows the results of the albedo scheme for the winter of 2016–2017 compared to the observed data. The simulated values closely matched the observed values, showing a generally consistent trend. Error analysis indicated an improvement over the separate calculations for each phase, with a MAE of 0.028, RMSE of 0.059, MAPE of 5.561%, and a notable increase in EF to 0.933.

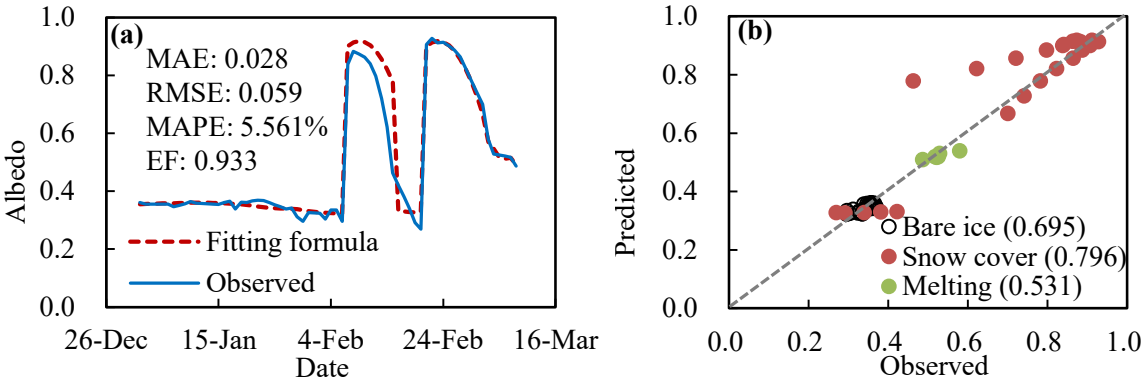


Figure 13. Observation and fitting results of the albedo in winter 2016–2017 (**a**) and the predicted vs. observed albedo (**b**), with the EF values calculated individually for each stage in parentheses.

4.2. Albedo Scheme Validation

To further validate the applicability of the albedo scheme (Equation (14)) for Lake Ulansu, portions of the albedo observation data from the winters of 2015–2016, 2017–2018, and 2022–2023 were used. For the bare ice and snow cover stage data, in contrast to the winter of 2016–2017, the snow on the ice surface was unevenly distributed due to wind effects, as shown in Figure 14. Among the three winters, only the winter of 2017–2018 had snow distribution data for beneath the sensors, recorded using drones. Therefore, for the winters of 2015–2016 and 2022–2023, only the observation data from the bare ice stages were used for validation, while the bare ice and snow cover stages were uniformly classified as the freezing stage.



Figure 14. Uneven snow distribution on the lake ice surface during the winter 2015–2016 (**a**) and 2017–2018 (**b**).

When the snow within the effective observation radius of the pyranometer is unevenly distributed, both the snow and the bare ice contribute to the albedo [3]. To assess the impact of this composite surface morphology on albedo, the snow cover proportion beneath the pyranometer was extracted from drone-recorded images of snow cover, as illustrated in

Figure 15. Based on the proportions of snow and bare ice, the albedo was calculated using Equation (15):

$$\text{Albedo} = S_s \times \alpha_s + S_i \times \alpha_i, \quad (15)$$

where S_s is the snow cover proportion, and S_i is the bare ice proportion.



Figure 15. Snow cover area within the effective radius (3 m) of the pyranometer on 16 January, 26 January, and 6 February 2018.

The albedo predicted by Equations (12)–(14), compared to the observed values, is shown in Figure 16, and the error analysis is presented in Table 6. For the predicted data from the freezing, melting, and entire stages, the MAE value was less than 0.05, with an average RMSE of 0.048 and MAPE of 10.793%. The EF for the freezing stage was 0.890, higher than the 0.826 for the melting stage. This difference was primarily due to observational limitations, because the data for the melting stage are mostly concentrated in the early stages of melting, which limits its ability to validate predictions for the later melting stages. After analyzing the data from both the freezing and melting stages, the overall EF reached 0.940, consistent with the results from the winter of 2016–2017.

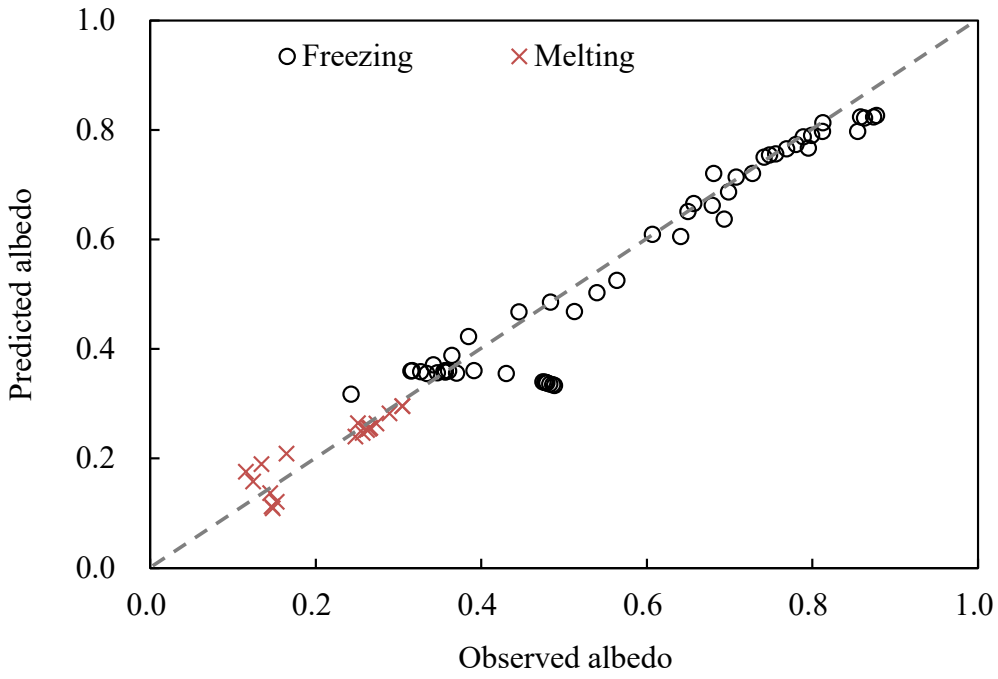


Figure 16. Observation and predicted results of the lake ice albedo.

Table 6. MAE, RMSE, MAPE, and EF for the scheme validation.

	MAE	RMSE	MAPE	EF
Freezing	0.041	0.062	8.607%	0.890
Melting	0.022	0.028	13.812%	0.826
All data	0.036	0.055	9.962%	0.940

5. Conclusions

Snow and ice albedos were measured on Lake Ulansu over a 68-day period during the winter of 2016–2017, alongside simultaneous atmospheric data observations. The observations were categorized into three distinct stages: bare ice, snow cover, and melting. The average albedo during the bare ice stage was 0.35, increasing to 0.91 following snowfall. The maximum ice thickness reached 46.4 cm, with two snowfall events occurring during the observation stage. The daily average temperature was −6.74 °C, with maximum and minimum temperatures of 0.44 and −14.73 °C, respectively. Due to the environmental conditions in arid and semi-arid regions, a sediment layer adhered to the ice surface, with an average sediment content of 1.39 g m^{-2}, showing a clear increasing trend.

Four existing albedo schemes (Gabison, SH, FB, and HS) were selected to predict the ice and snow albedo on Lake Ulansu during the winter of 2016–2017. During the bare ice stage, the predicted albedo trend showed the opposite to the observed trend, primarily due to the increasing sediment content on the ice surface. The HS II scheme performed the best for predicting snow cover albedo, achieving an EF of 0.55. For the melting stage, none of the existing schemes were suitable for accurately predicting albedo.

A new albedo scheme for ice and snow was developed based on the observed data and existing schemes. For the bare ice stage, the parameter of sediment content on the lake ice surface, which had not been considered in the previous surface albedo schemes, was incorporated into the new scheme. To enhance its applicability, the sediment content was integrated into the new scheme in the form of a function of ice thickness. This albedo scheme was derived from the SH scheme and had an EF of 0.695. The HS II scheme was adapted to develop the snow cover albedo scheme, with an EF of 0.796. The albedo scheme for the melting stage was based on the ice thickness and observed albedo data, with an EF of 0.531. Integration of the schemes for all three stages produced a comprehensive albedo scheme for Lake Ulansu, with an overall EF of 0.933. The albedo scheme was validated using albedo observation data from the winters of 2015–2016, 2017–2018, and 2022–2023, achieving an EF of 0.940 when comparing predicted and observed values. Validation analysis showed that the new albedo scheme closely matched the observed lake ice and snow albedo on Lake Ulansu. During the validation process, it was found that when snow is unevenly distributed, the contribution of bare ice to the albedo should also be considered alongside the snow. Therefore, more wind and snow cover data are needed to establish general patterns of blowing snow cover on Lake Ulansu, which would further improve the applicability of the new scheme.

The new albedo scheme has potential applicability for snow and ice that encounter surface sediment during winter in the Central Asian arid climate zone. However, additional field observation data are required to develop a more generalized parameterization formula for sediment content on the ice surface, such as examining its potential relationship with wind, and the contribution of sediment content in snow to albedo changes. Moreover, further field data are needed to validate the applicability of this albedo scheme for other lakes in the Central Asian arid climate zone. Additionally, we will include a comparative study of the measured and predicted albedo with satellite-derived data to enhance the accuracy and robustness of the scheme. These aspects should be key focuses of future research.

Author Contributions: Conceptualization, X.C.; investigation, X.C. and P.H.; writing—original draft preparation, X.C. and P.L.; writing—review and editing, M.Y., B.C., W.G., X.S., and L.W. All authors have read and agreed to the published version of the manuscript.

Funding: This research was supported by the Qingdao Huanghai University Doctoral Research Fund Project (2024boshi02, 2024boshi03, 2022boshi03), the National Natural Science Foundation of China (42406244, U24A20582), the Postdoctoral Fellowship Program of CPSF (Grant number GZB20230102), the Joint Funds of the National Natural Science Foundation of Liaoning Province (2023-BSBA-021), the Shandong Provincial Natural Science Foundation (ZR2024QD256), the Qingdao City Natural Science Foundation (24-4-4-zrjj-48-jch), and the 2024 Shandong Province College Students Innovation and Entrepreneurship Training Program Project (S202413320023).

Data Availability Statement: The data presented in this study are available on request from the corresponding authors.

Acknowledgments: The authors would like to thank the research group from Water Conservancy and Civil Engineering College (Inner Mongolia Agricultural University), for their contributions to the in-situ measurement.

Conflicts of Interest: Author Lijun Wang was employed by the company Huacheng Boyuan Engineering Technology Group Co., Ltd. The remaining authors declare that the research was conducted in the absence of any commercial or financial relationships that could be construed as a potential conflict of interest.

Abbreviations

The following abbreviations are used in this manuscript:

SH	Shine and Henderson-Sellers
FB	Flato and Brown
HS	Henneman and Stefan
MAE	Mean absolute error
RMSE	Root mean square error
MAPE	Mean absolute percent error
EF	Modeling efficiency

Appendix A

Error calculation formulas:

Mean absolute error (MAE):

$$\mathrm{MAE} = \frac{(\sum|y_i - \hat{y}_i|)}{n},$$

Root mean square error (RMSE):

$$\mathrm{RMSE} = \sqrt{\frac{\sum(y_i - \hat{y}_i)^2}{n}},$$

Mean absolute percent error (MAPE):

$$\mathrm{MAPE} = \frac{1}{n}\sum\left|\frac{y_i - \hat{y}_i}{y_i}\right|,$$

Modeling efficiency (EF):

$$\mathrm{EF} = 1 - \frac{\sum(y_i - \hat{y}_i)^2}{\sum(y_i - \bar{y})^2},$$

where y_i is the observed value, $\hat{y}_i$ is the simulated value, and n is the number of data points.

References

1. Austin, J.A.; Colman, S.M. Lake Superior summer water temperatures are increasing more rapidly than regional air temperatures: A positive ice-albedo feedback. *Geophys. Res. Lett.* **2007**, *34*, L06604. [CrossRef]
2. Robinson, A.L.; Ariano, S.S.; Brown, L.C. The influence of snow and ice albedo towards improved lake ice simulations. *Hydrology* **2021**, *8*, 11. [CrossRef]
3. Cao, X.; Lu, P.; Leppäranta, M.; Arvola, L.; Huotari, J.; Shi, X.; Li, G.; Li, Z. Solar radiation transfer for an ice-covered lake in the central Asian arid climate zone. *Inland Waters* **2021**, *11*, 89–103. [CrossRef]
4. Lang, J.; Lyu, S.; Li, Z.; Ma, Y.; Su, D. An investigation of ice surface albedo and its influence on the high-altitude lakes of the Tibetan Plateau. *Remote Sens.* **2018**, *10*, 218. [CrossRef]
5. Raoult, N.; Charbit, S.; Dumas, C.; Maignan, F.; Ottlé, C.; Bastrikov, V. Improving modelled albedo over the Greenland ice sheet through parameter optimisation and MODIS snow albedo retrievals. *Cryosphere* **2023**, *17*, 2705–2724. [CrossRef]
6. Shao, D.; Jin, Y.; Ji, W.; Li, H.; Feng, T.; Li, H.; Wang, J.; Hao, X. Estimating broadband snow albedo by an asymptotic radiative transfer model-constrained deep learning models. *IEEE Trans. Geosci. Remote Sens.* **2024**, *62*, 4302016. [CrossRef]
7. Brown, L.C.; Duguay, C.R. The response and role of ice cover in lake-climate interactions. *Prog. Phys. Geogr.* **2010**, *34*, 671–704. [CrossRef]
8. Leppäranta, M. *Freezing of Lakes and the Evolution of Their Ice Cover*; Springer: Berlin/Heidelberg, Germany, 2015.
9. Benson, B.J.; Magnuson, J.J.; Jensen, O.P.; Card, V.M.; Hodgkins, G.; Korhonen, J.; Livingstone, D.M.; Stewart, K.M.; Weyhenmeyer, G.A.; Granin, N.G. Extreme events, trends, and variability in Northern Hemisphere lake-ice phenology (1855–2005). *Clim. Change* **2012**, *112*, 299–323. [CrossRef]
10. Sharma, S.; Richardson, D.C.; Woolway, R.I.; Imrit, M.A.; Bouffard, D.; Blagrave, K.; Daly, J.; Filazzola, A.; Granin, N.; Korhonen, J. Loss of ice cover, shifting phenology, and more extreme events in Northern Hemisphere lakes. *J. Geophys. Res. Biogeosci.* **2021**, *126*, e2021JG006348. [CrossRef]
11. Sharma, S.; Blagrave, K.; Filazzola, A.; Imrit, M.A.; Hendricks Franssen, H.J. Forecasting the permanent loss of lake ice in the Northern Hemisphere within the 21st century. *Geophys. Res. Lett.* **2021**, *48*, e2020GL091108. [CrossRef]
12. Shuter, B.; Minns, C.K.; Fung, S.R. Empirical models for forecasting changes in the phenology of ice cover for Canadian lakes. *Can. J. Fish. Aquat. Sci.* **2013**, *70*, 982–991. [CrossRef]
13. Leppäranta, M. Modelling the formation and decay of lake ice. In *The Impact of Climate Change on European Lakes*; Springer: Berlin/Heidelberg, Germany, 2010; pp. 63–83.
14. Knoll, L.B.; Sharma, S.; Denfeld, B.A.; Flaim, G.; Hori, Y.; Magnuson, J.J.; Straile, D.; Weyhenmeyer, G.A. Consequences of lake and river ice loss on cultural ecosystem services. *Limnol. Oceanogr. Lett.* **2019**, *4*, 119–131. [CrossRef]
15. Hampton, S.E.; Galloway, A.W.; Powers, S.M.; Ozersky, T.; Woo, K.H.; Batt, R.D.; Labou, S.G.; O'Reilly, C.M.; Sharma, S.; Lottig, N.R. Ecology under lake ice. *Ecol. Lett.* **2017**, *20*, 98–111. [CrossRef] [PubMed]
16. Lioubimtseva, E.; Cole, R. Uncertainties of climate change in arid environments of Central Asia. *Rev. Fish. Sci.* **2006**, *14*, 29–49. [CrossRef]
17. Yu, Y.; Pi, Y.; Yu, X.; Ta, Z.; Sun, L.; Disse, M.; Zeng, F.; Li, Y.; Chen, X.; Yu, R. Climate change, water resources and sustainable development in the arid and semi-arid lands of Central Asia in the past 30 years. *J. Arid Land* **2019**, *11*, 1–14. [CrossRef]
18. Huang, W.; Zhao, W.; Zhang, C.; Leppäranta, M.; Li, Z.; Li, R.; Lin, Z. Sunlight penetration dominates the thermal regime and energetics of a shallow ice-covered lake in arid climate. *Cryosphere* **2022**, *16*, 1793–1806. [CrossRef]
19. Yang, Y.; Leppäranta, M.; Cheng, B.; Li, Z. Numerical modelling of snow and ice thicknesses in Lake Vanajavesi, Finland. *Tellus A Dyn. Meteorol. Oceanogr.* **2012**, *64*, 17202. [CrossRef]
20. You, Y.; An, L.; Li, S.; Zhang, B.; Zhang, J. Analysis and Research on the Differences in Observed Data of Sand–Dust Weather between China and Mongolia. *Atmosphere* **2023**, *14*, 1401. [CrossRef]
21. Fang, Y.; Changyou, L.; Leppäranta, M.; Xiaonghong, S.; Shengnan, Z.; Chengfu, Z. Notable increases in nutrient concentrations in a shallow lake during seasonal ice growth. *Water Sci. Technol.* **2016**, *74*, 2773–2783. [CrossRef]
22. Conway, H.; Gades, A.; Raymond, C. Albedo of dirty snow during conditions of melt. *Water Resour. Res.* **1996**, *32*, 1713–1718. [CrossRef]
23. Grenfell, T.C.; Warren, S.G.; Mullen, P.C. Reflection of solar radiation by the Antarctic snow surface at ultraviolet, visible, and near-infrared wavelengths. *J. Geophys. Res. Atmos.* **1994**, *99*, 18669–18684. [CrossRef]
24. Dirmhirn, I.; Eaton, F.D. Some characteristics of the albedo of snow. *J. Appl. Meteorol. (1962–1982)* **1975**, *14*, 375–379. [CrossRef]
25. Bergstrom, A.; Gooseff, M.N.; Myers, M.; Doran, P.T.; Cross, J.M. The seasonal evolution of albedo across glaciers and the surrounding landscape of Taylor Valley, Antarctica. *Cryosphere* **2020**, *14*, 769–788. [CrossRef]
26. Jakkila, J.; Leppäranta, M.; Kawamura, T.; Shirasawa, K.; Salonen, K. Radiation transfer and heat budget during the ice season in Lake Pääjärvi, Finland. *Aquat. Ecol.* **2009**, *43*, 681–692. [CrossRef]
27. Leppäranta, M.; Terzhevik, A.; Shirasawa, K. Solar radiation and ice melting in Lake Vendyurskoe, Russian Karelia. *Hydrol. Res.* **2010**, *41*, 50–62. [CrossRef]

28. Chen, Q.-X.; Gao, Z.-Y.; Huang, C.-L.; Dong, S.-K.; Lin, K.-F. Simulation of Spectral Albedo and Bidirectional Reflectance over Snow-Covered Urban Canyon: Model Development and Factor Analysis. *Remote Sens.* **2024**, *16*, 2340. [CrossRef]
29. Li, Z.; Wang, Q.; Tang, M.; Lu, P.; Li, G.; Leppäranta, M.; Huotari, J.; Arvola, L.; Shi, L. Diurnal cycle model of lake ice surface albedo: A case study of Wuliangsuhai Lake. *Remote Sens.* **2021**, *13*, 3334. [CrossRef]
30. Henneman, H.E.; Stefan, H.G. Albedo models for snow and ice on a freshwater lake. *Cold Reg. Sci. Technol.* **1999**, *29*, 31–48. [CrossRef]
31. Rogers, C.K.; Lawrence, G.A.; Hamblin, P.F. Observations and numerical simulation of a shallow ice-covered midlatitude lake. *Limnol. Oceanogr.* **1995**, *40*, 374–385. [CrossRef]
32. Brock, B.W.; Willis, I.C.; Sharp, M.J. Measurement and parameterization of albedo variations at Haut Glacier d'Arolla, Switzerland. *J. Glaciol.* **2000**, *46*, 675–688. [CrossRef]
33. Pedersen, C.A.; Winther, J.-G. Intercomparison and validation of snow albedo parameterization schemes in climate models. *Clim. Dyn.* **2005**, *25*, 351–362. [CrossRef]
34. Gray, D.; Landine, P. Albedo model for shallow prairie snow covers. *Can. J. Earth Sci.* **1987**, *24*, 1760–1768. [CrossRef]
35. Flato, G.M.; Brown, R.D. Variability and climate sensitivity of landfast Arctic sea ice. *J. Geophys. Res. Ocean.* **1996**, *101*, 25767–25777. [CrossRef]
36. Gabison, R. A thermodynamic model of the formation, growth, and decay of first-year sea ice. *J. Glaciol.* **1987**, *33*, 105–119. [CrossRef]
37. Shine, K.; Henderson, S. The sensitivity of a thermodynamic sea ice model to changes in surface albedo parameterization. *J. Geophys. Res. Atmos.* **1985**, *90*, 2243–2250. [CrossRef]
38. Gardner, A.S.; Sharp, M.J. A review of snow and ice albedo and the development of a new physically based broadband albedo parameterization. *J. Geophys. Res. Earth Surf.* **2010**, *115*, F01009. [CrossRef]
39. Lu, P.; Cao, X.; Li, G.; Huang, W.; Leppäranta, M.; Arvola, L.; Huotari, J.; Li, Z. Mass and heat balance of a lake ice cover in the central Asian arid climate zone. *Water* **2020**, *12*, 2888. [CrossRef]
40. Shi, X.; Yu, H.; Zhao, S.; Sun, B.; Liu, Y.; Huo, J.; Wang, S.; Wang, J.; Wu, Y.; Wang, Y. Impacts of environmental factors on Chlorophyll-a in lakes in cold and arid regions: A 10-year study of Wuliangsuhai Lake, China. *Ecol. Indic.* **2023**, *148*, 110133. [CrossRef]
41. Huang, W.; Zhang, Z.; Li, Z.; Leppäranta, M.; Arvola, L.; Song, S.; Huotari, J.; Lin, Z. Under-ice dissolved oxygen and metabolism dynamics in a shallow lake: The critical role of ice and snow. *Water Resour. Res.* **2021**, *57*, e2020WR027990. [CrossRef]
42. Zhang, X.; Zhang, C.; Meng, F.; Wang, C.; Ren, P.; Zou, Q.; Luan, J. Near-zero liquid discharge of desulfurization wastewater by electrodialysis-reverse osmosis hybrid system. *J. Water Process Eng.* **2021**, *40*, 101962. [CrossRef]
43. Maykut, G.A. Large-scale heat exchange and ice production in the central Arctic. *J. Geophys. Res. Ocean.* **1982**, *87*, 7971–7984. [CrossRef]
44. Heron, R.; Woo, M.-K. Decay of a High Arctic lake-ice cover: Observations and modelling. *J. Glaciol.* **1994**, *40*, 283–292. [CrossRef]

Disclaimer/Publisher's Note: The statements, opinions and data contained in all publications are solely those of the individual author(s) and contributor(s) and not of MDPI and/or the editor(s). MDPI and/or the editor(s) disclaim responsibility for any injury to people or property resulting from any ideas, methods, instructions or products referred to in the content.